Electronic Supporting Information

Exploring the multifunctionality in metal-organic frameworks materials: how do the stilbenedicarboxylate and imidazolyl ligands tune the characteristics of coordination polymers?

Marina O. Barsukova,[a,b] Sergey A. Sapchenko,*[a,b,c] Konstantin A. Kovalenko,[a,b] Denis G. Samsonenko,[a,b] Andrei S. Potapov,[d] Danil N. Dybtsev,[a,b] Vladimir P. Fedin[a,b]

[a] *Nikolaev Institute of Inorganic Chemistry, Siberian Branch of the Russian Academy of Sciences, Acad. Lavrentieva Ave., 3, 630090, Novosibirsk, Russia*

[b] *Novosibirsk State University, Pirogova st., 2, 630090, Novosibirsk, Russia*

[c] *School of Chemistry, University of Manchester, Oxford Road, Manchester, M13 9PL, U.K.*

[d] *National Research Tomsk Polytechnic University, Lenin Ave., 30, 634050, Tomsk, Russia*

* *Corresponding author at: Nikolaev Institute of Inorganic Chemistry, Siberian Branch of the Russian Academy of Sciences, Akad. Lavrentiev Ave., 3, 630090 Novosibirsk, Russia.*
Tel.: +7 383 330 9490; fax: +7 383 330 9489.

X-ray crystallography. The fragments of the coordination polymers with disorders for compounds **1**, **2**, **3**, **4**, **5** and **6** in thermal ellipsoid mode are presented in Figures S1, S3, S5, S7, S9 and S11, respectively. Additional figures, highlighting the inner surfaces of the frameworks **1**, **2**, **3**, **4**, **4a**, **5** and **6** are presented in Fig. S2, S4, S6, S8, S8a, S10 and S12, respectively.

Thermogravimetric analyses. The TGA plots for the reported compounds are presented in Fig. S13-S14. The TGA plots for the I_2-adsorbed and activated compounds **2** and **5** are presented in Fig. S15–S16.

Powder X-ray diffraction analyses. The PXRD data for the as-synthesythed and activated compounds **1**, **2**, **3**, **4**, **5** and **6** are presented on Fig. S17–S22. For the compound **2** and **5** powder X-ray diffraction (PXRD) patterns with adsorbed I_2 are presented in Fig. S23–S24.

N_2 adsorption isotherm measurements. The analyses were performed on Quantochrome's Autosorb iQ at 77K. The gas adsorption/desorption isotherms for the activated compounds **1-6** are provided on Fig.S25.

I_2 sorption from solution. The photos show sample color of activated compound **2** and samples soaked in I_2 solution in methanol, toluene and CH_2Cl_2 for 1 day in Fig. S26.

Raman spectroscopy. The Raman spectra of the activated and I_2-adsorbed compounds **2** and **5** are present in Fig. S27.

Luminescent properties. Normalized spectra of emission (λ_{ex} = 390 nm) and excitation of obtained as-synthesized and activated compounds, and free H_2sdc are shown on Fig. S28.

Tables. Single crystal X-ray crystallography data and literature references for luminescent properties.

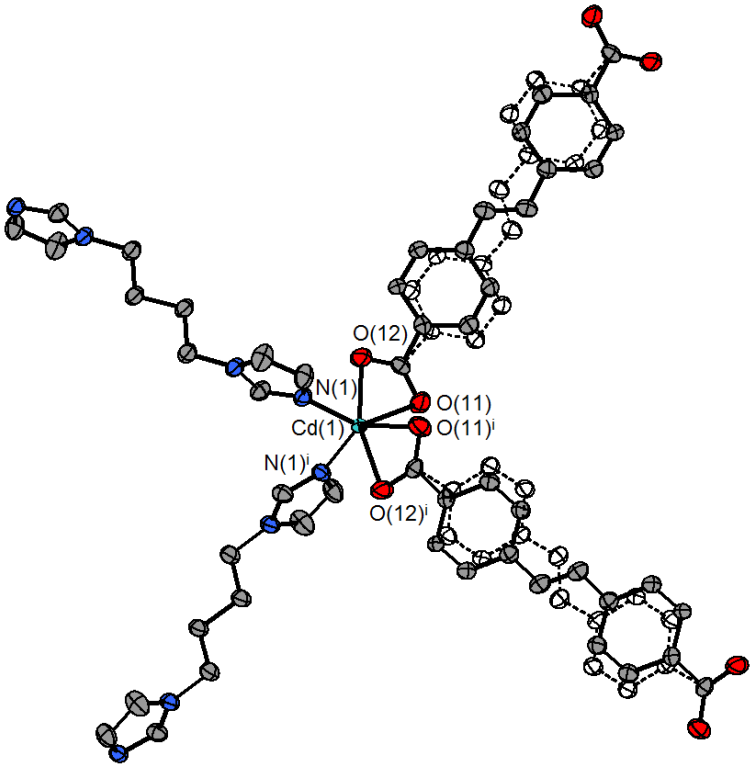

Figure S1. View of node in **1** (hydrogen atoms are omitted; ellipsoids are at the 50% probability level). Symmetry codes for related atoms: i) $1 - x, y, 1.5 - z$.

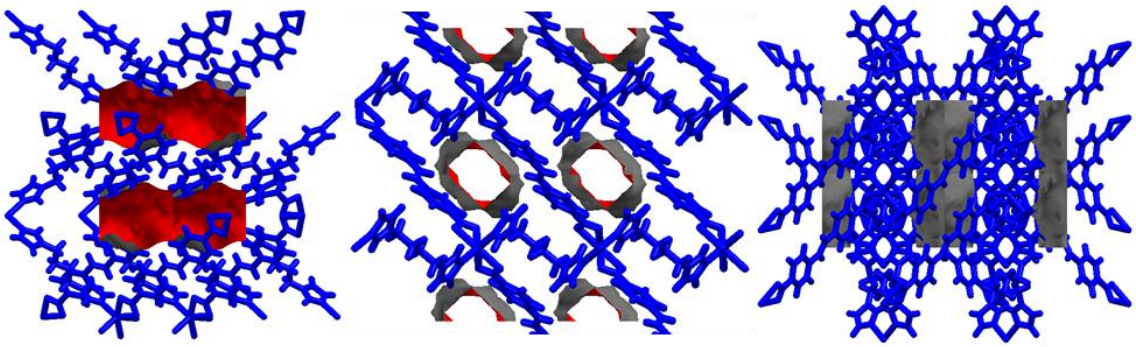

Figure S2. Calculated void surfaces for **1** along *a* (left), *b* (center) and *c* axis (right).

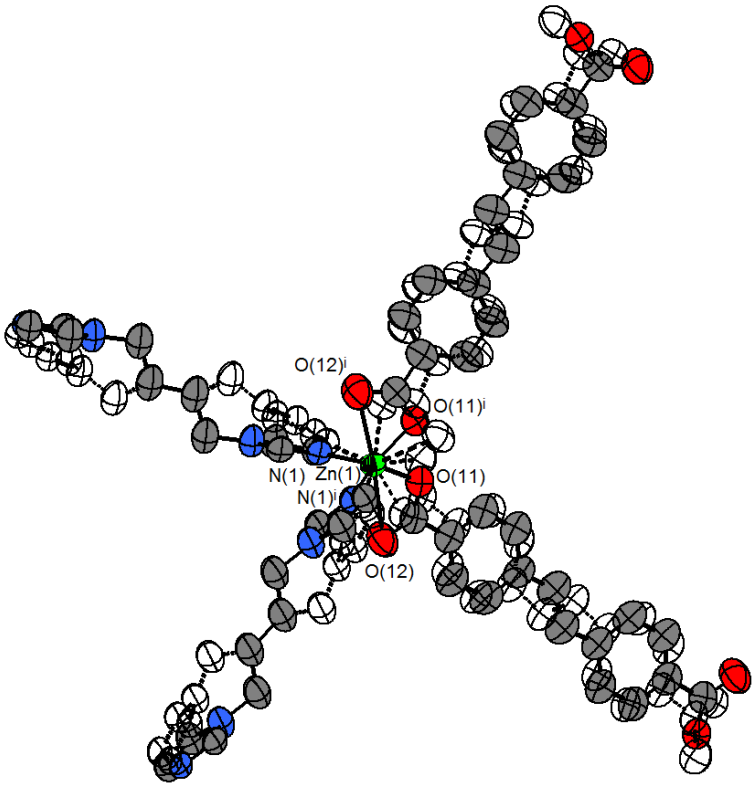

Figure S3. View of node in **2** (hydrogen atoms are omitted; ellipsoids are at the 50% probability level). Symmetry codes for related atoms: i) $-x, y, 1.5-z$.

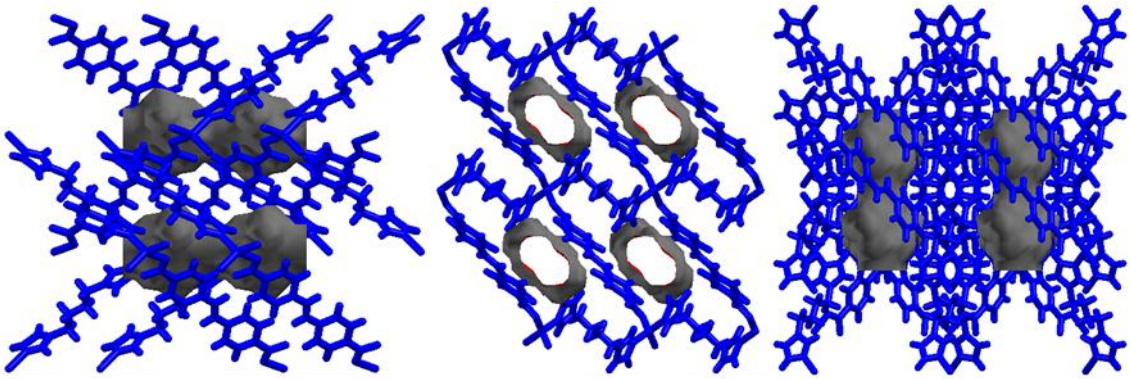

Figure S4. Calculated void surfaces for **2** along *a* (left), *b* (center) and *c* axis (right).

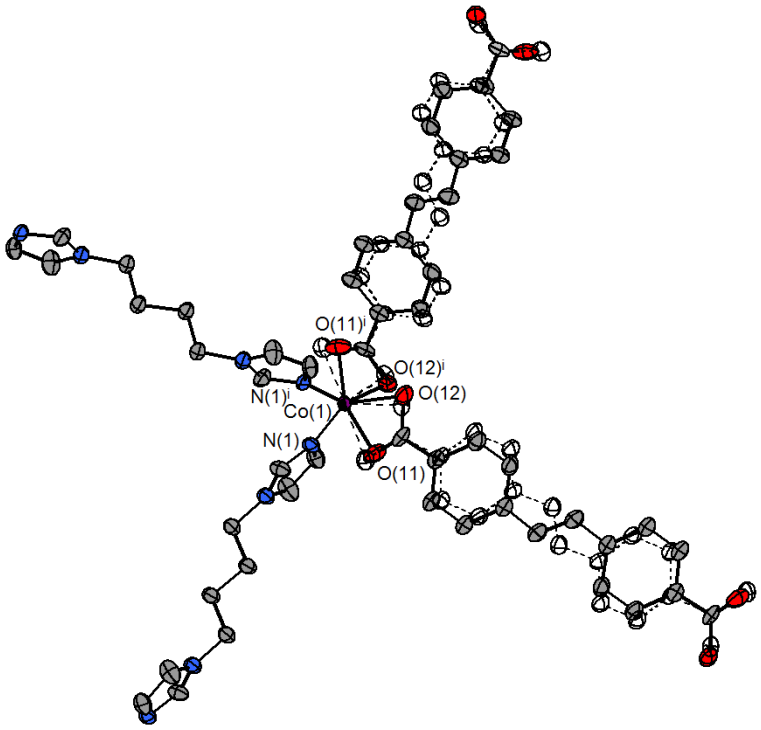

Figure S5. View of node in **3** (hydrogen atoms are omitted; ellipsoids are at the 50% probability level). Symmetry codes for related atoms: i) $1 - x, y, 1.5 - z$.

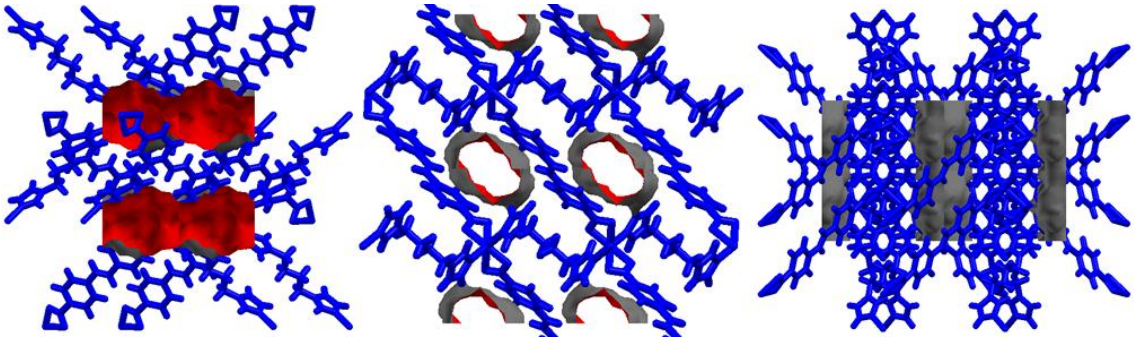

Figure S6. Calculated void surfaces for **3** along *a* (left), *b* (center) and *c* axis (right).

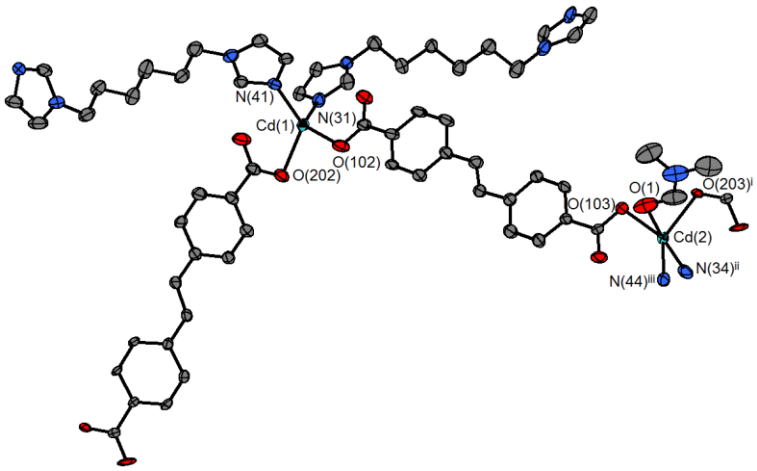

Figure S7. View of node in **4** (hydrogen atoms are omitted; ellipsoids are at the 50% probability level). Symmetry codes for related atoms: i) − 2 + *x*, − 1 + *y*, z; ii) 1.5 − *x*, − *y*, − 0.5 + *z*; iii) − 0.5 − *x*, 1 − *y*, − 0.5 + *z*.

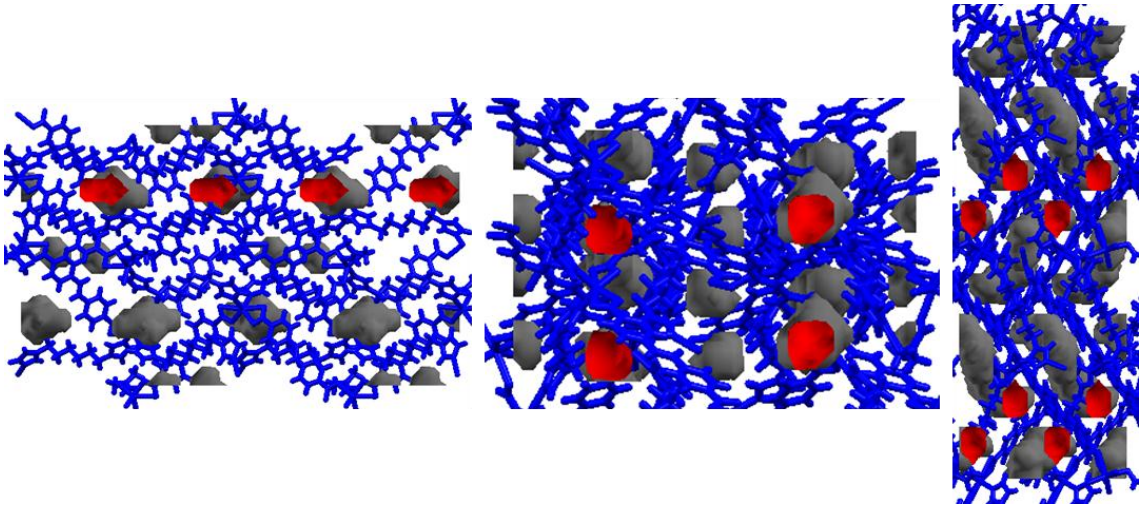

Figure S8. Calculated void surfaces for **4** along *a* (left), *b* (center) and *c* axis (right).

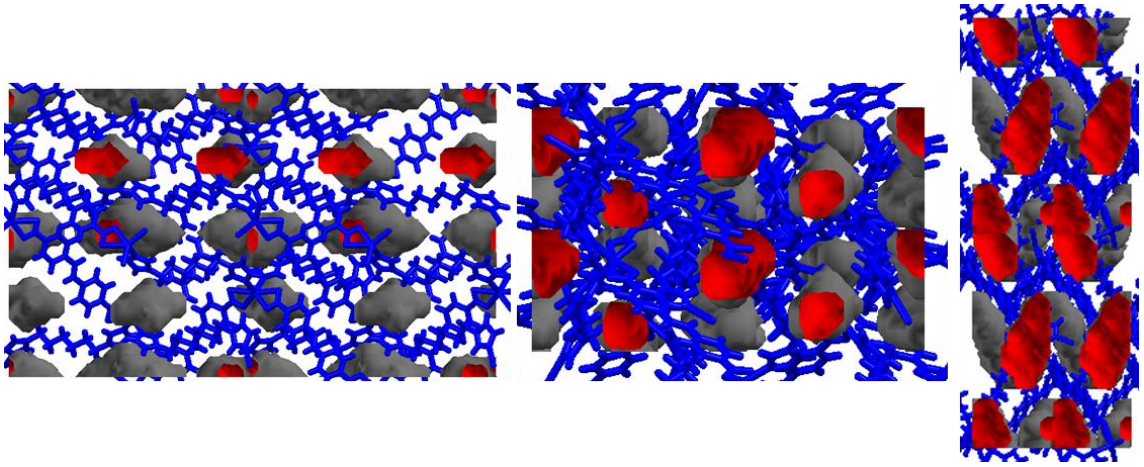

Figure S8a. Calculated void surfaces for **4a** along *a* (left), *b* (center) and *c* axis (right).

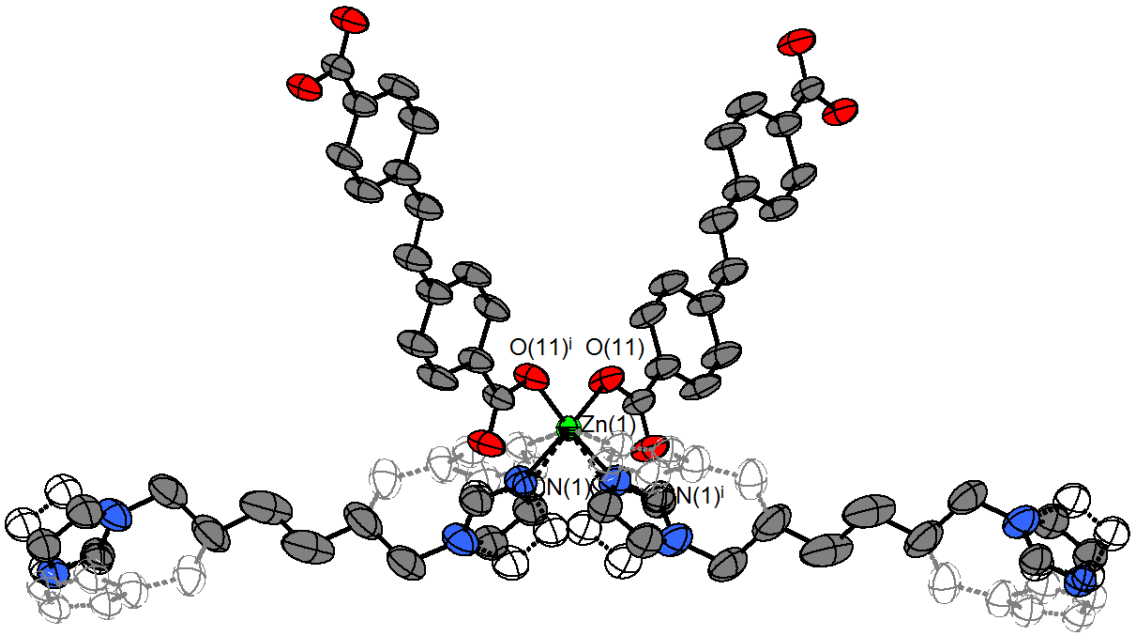

Figure S9. View of node in **5** (hydrogen atoms are omitted; ellipsoids are at the 50% probability level). Symmetry codes for related atoms: i) $1 - x, y, 1.5 - z$.

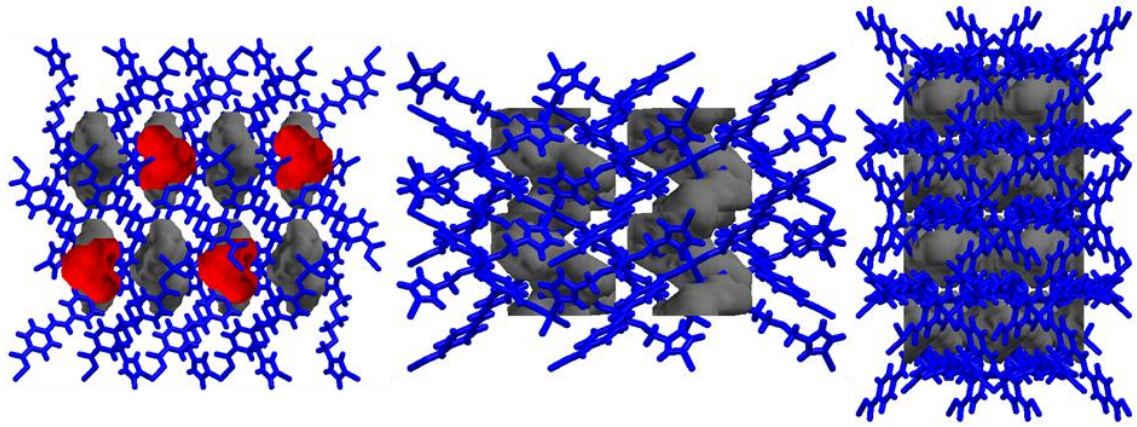

Figure S10. Calculated void surfaces for **5** along *a* (left), *b* (center) and *c* axis (right).

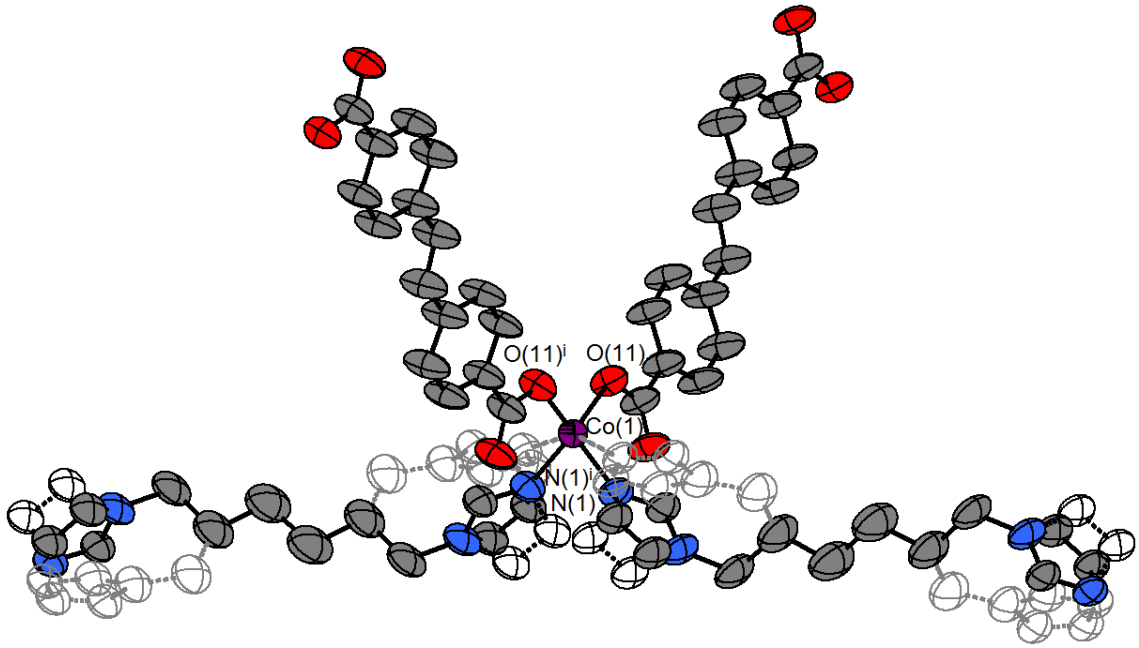

Figure S11. View of node in **6** (hydrogen atoms are omitted; ellipsoids are at the 50% probability level). Symmetry codes for related atoms: i) $1 - x, y, 0.5 - z$.

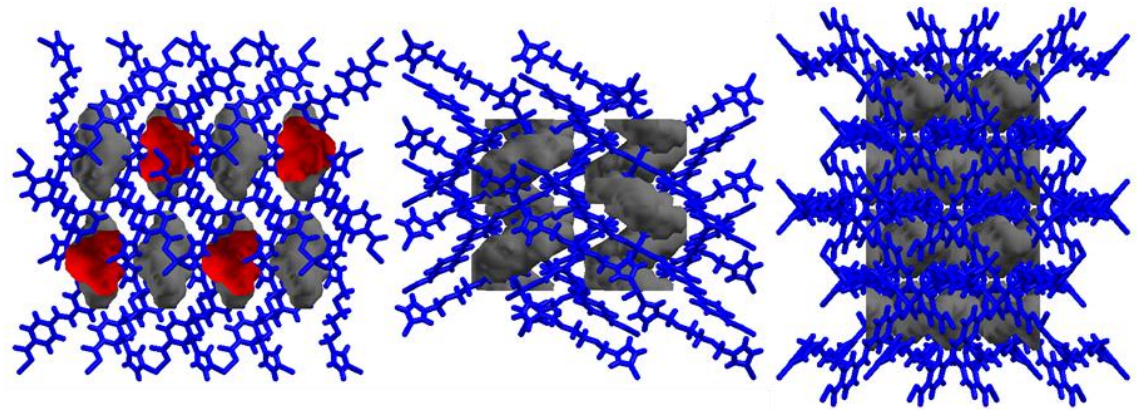

Figure S12. Calculated void surfaces for **6** along *a* (left), *b* (center) and *c* axis (right).

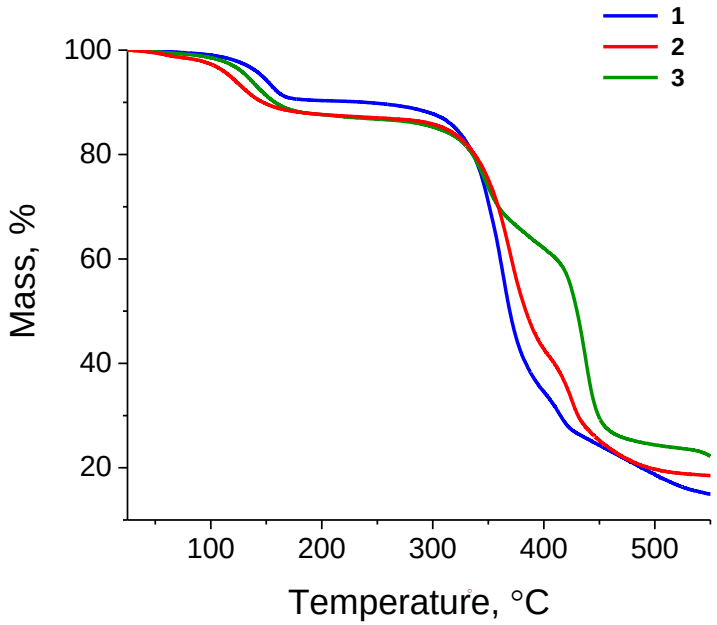

Figure S13. TGA plots for **1**, **2** and **3**.

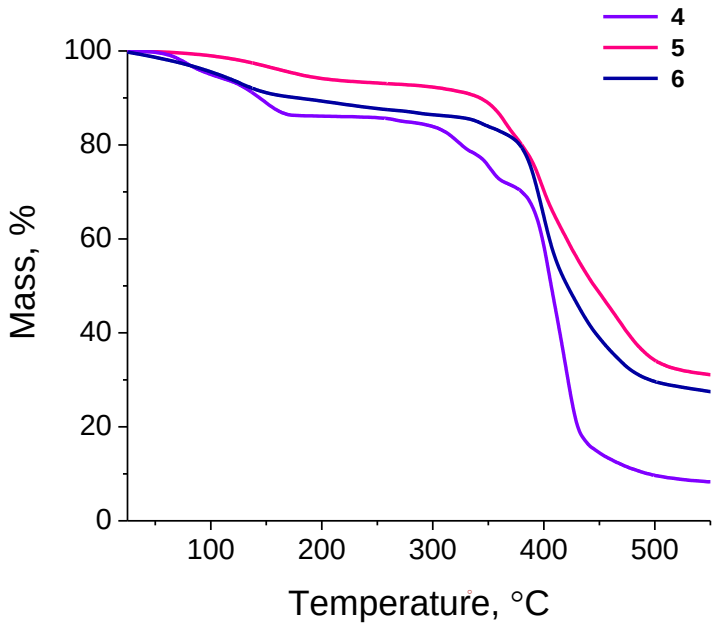

Figure S14. TGA plots for **4**, **5** and **6**.

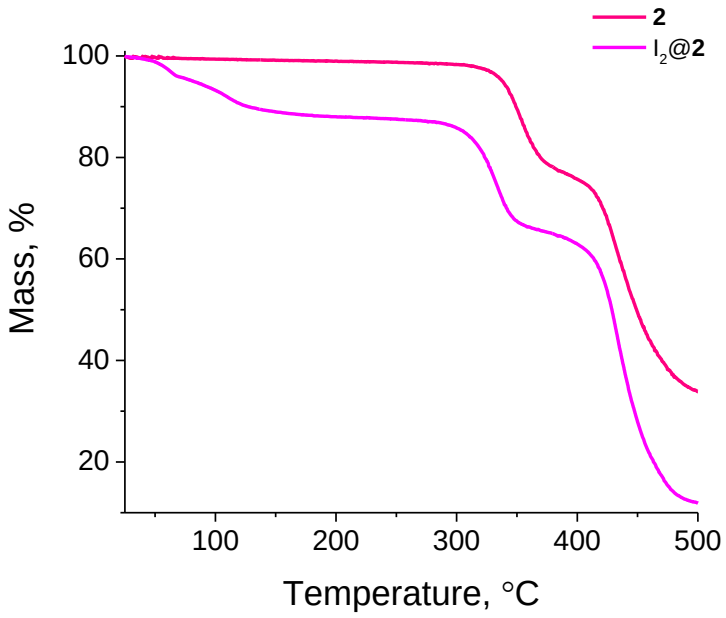

Figure S15. TGA plots for activated **2** and I_2-loaded sample of **2**.

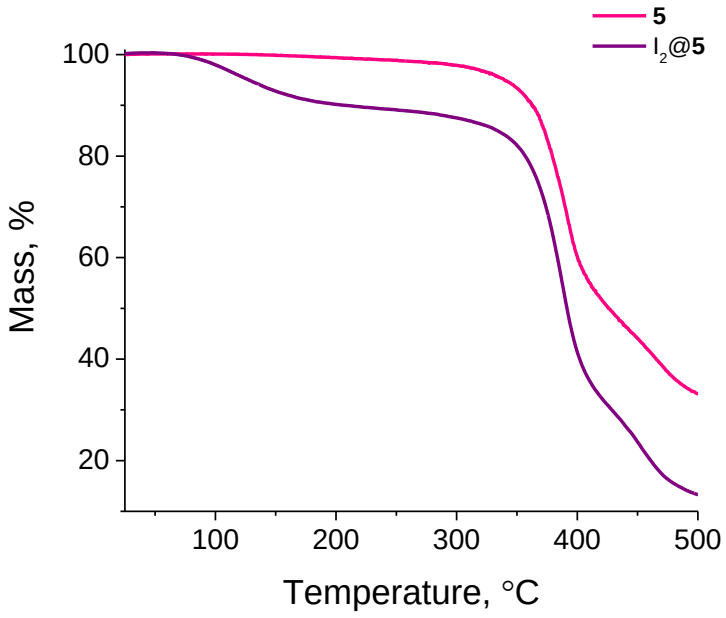

Figure S16. TGA plots for activated **5** and I_2-loaded sample of **5**.

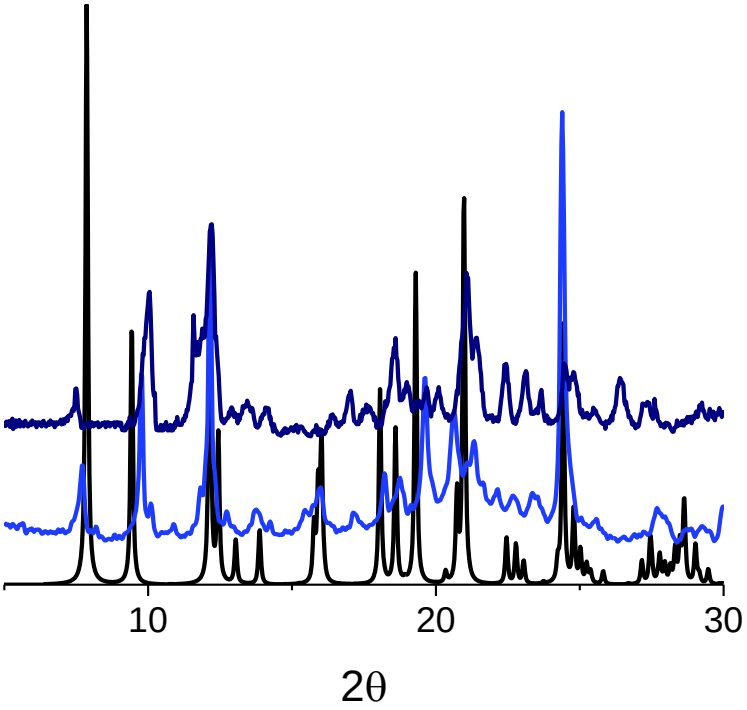

Figure S17. PXRD pattern of calculated for **1** (black) in comparison with patterns of as-synthesized **1** (blue), and activated **1** (dark blue).

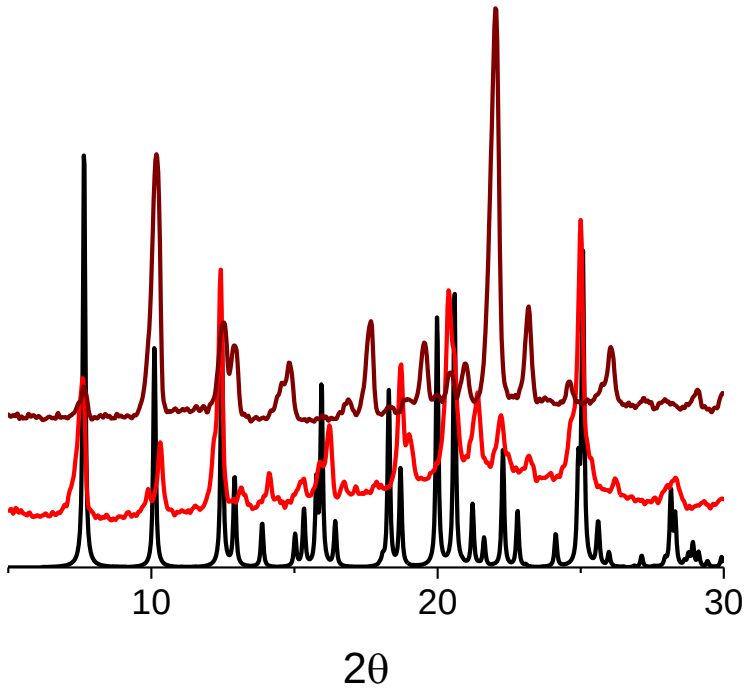

Figure S18. PXRD pattern of calculated for **2** (black) in comparison with patterns of as-synthesized **2** (red), and activated **2** (dark red).

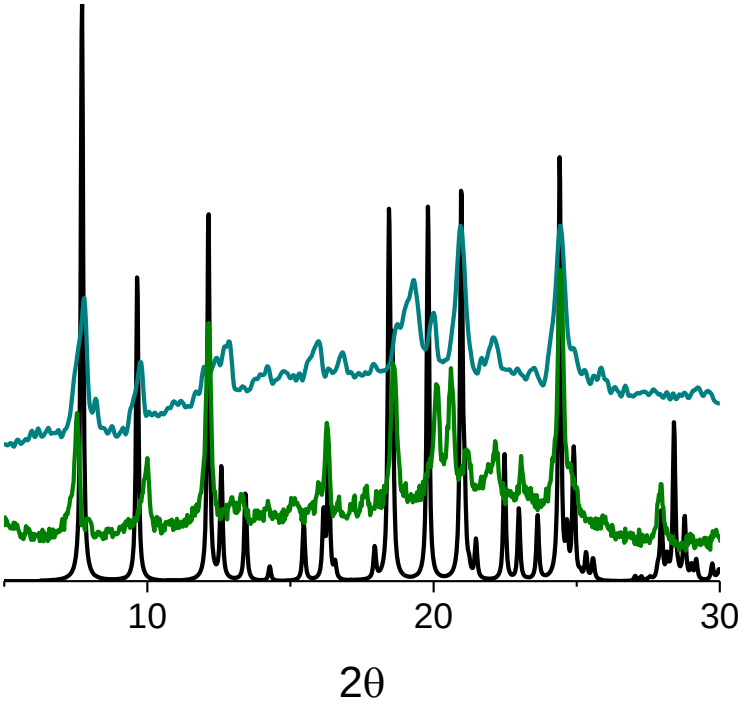

Figure S19. PXRD pattern of calculated for **3** (black) in comparison with patterns of as-synthesized **3** (green), and activated **3** (dark green).

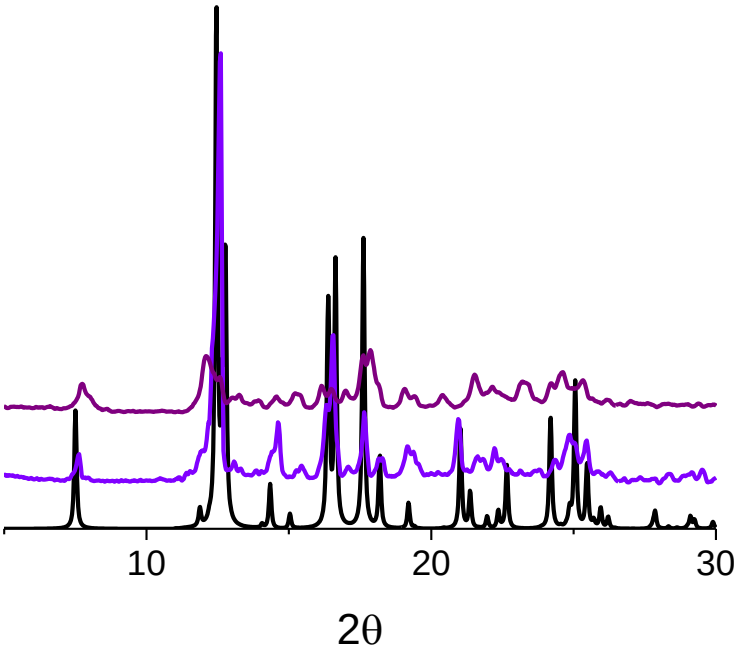

Figure S20. PXRD pattern of calculated for **4** (black) in comparison with patterns of as-synthesized **4** (violet), and activated **4** (dark violet).

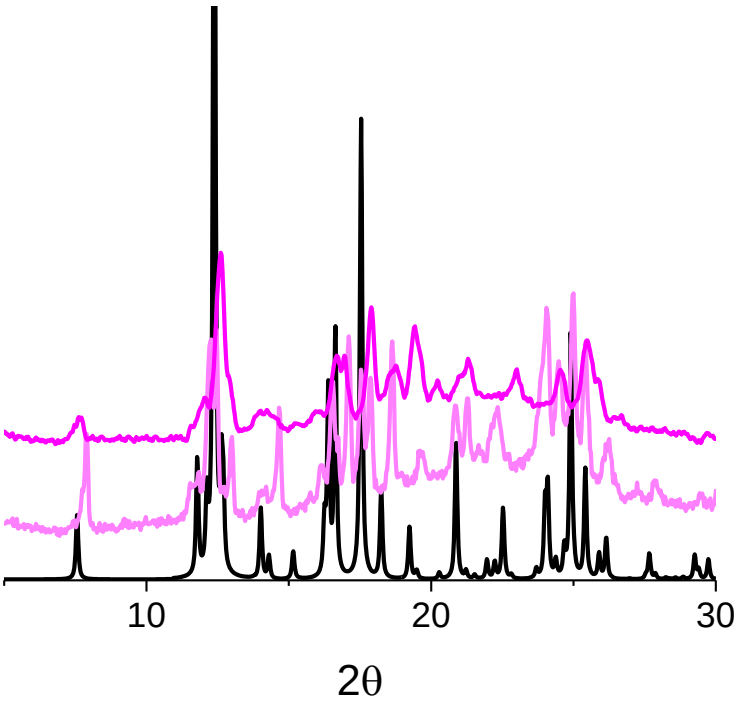

Figure S21. PXRD pattern of calculated for **5** (black) in comparison with patterns of as-synthesized **5** (light magenta), and activated **5** (magenta).

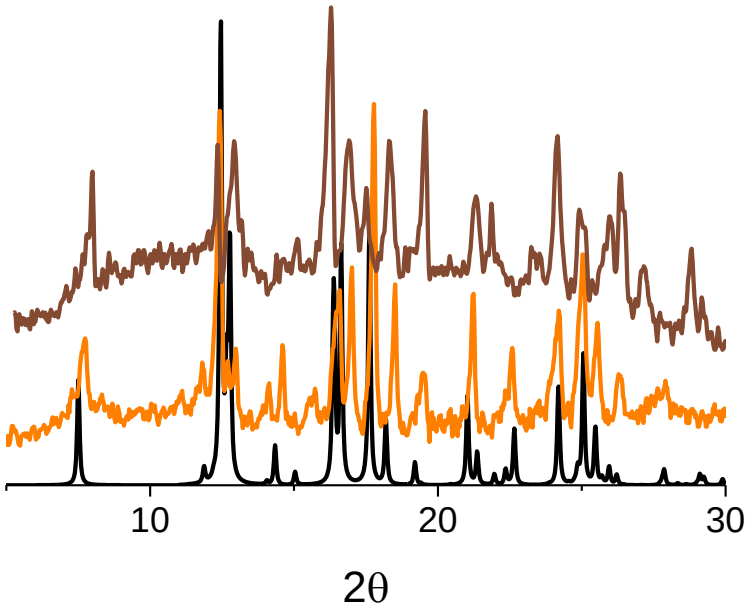

Figure S22. PXRD pattern of calculated for **6** (black) in comparison with patterns of as-synthesized **6** (orange), and activated **6** (brown).

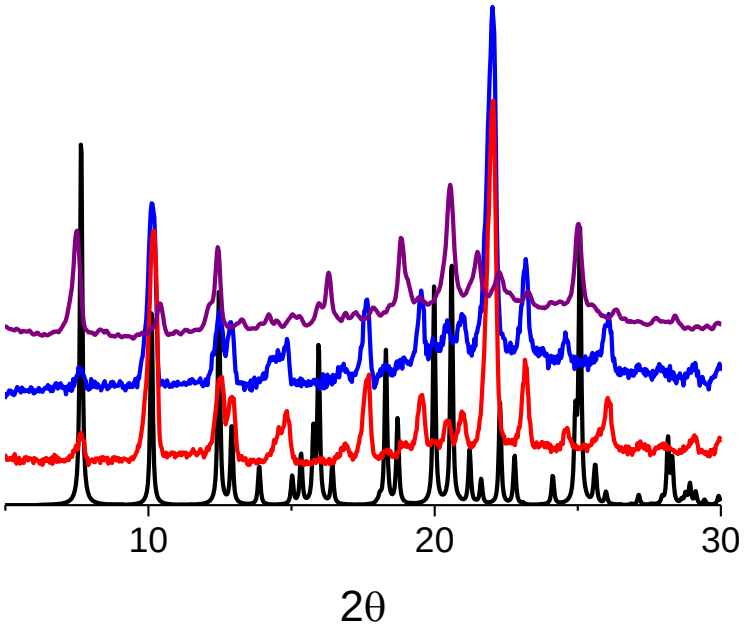

Figure S23. PXRD pattern of calculated for **2** (black) in comparison with patterns of activated **2** (red), **2** with I_2 adsorbed (blue) and **2** after I_2 desorption in methanol (purple).

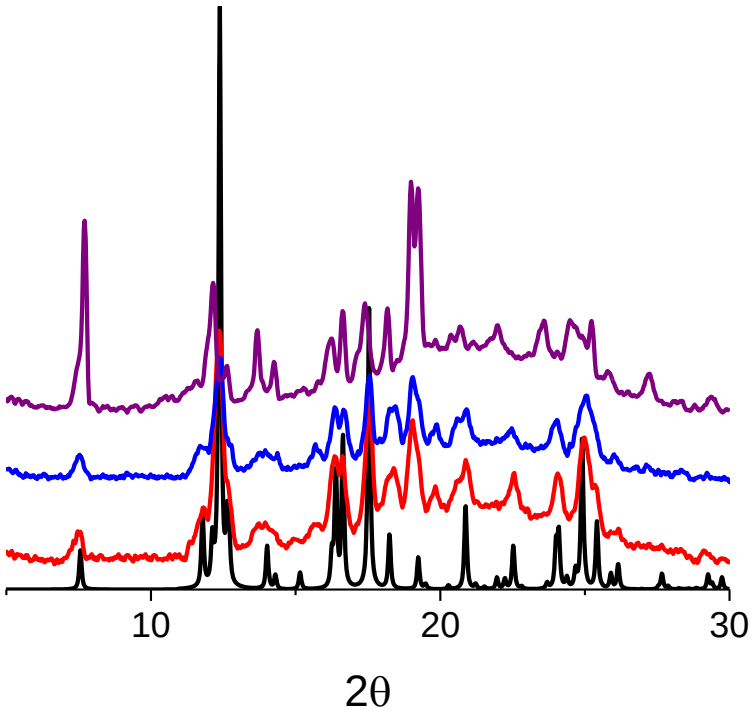

Figure S24. PXRD pattern of calculated for **5** (black) in comparison with patterns of activated **5** (red), **5** with I_2 adsorbed (blue) and **5** after I_2 desorption in methanol (purple).

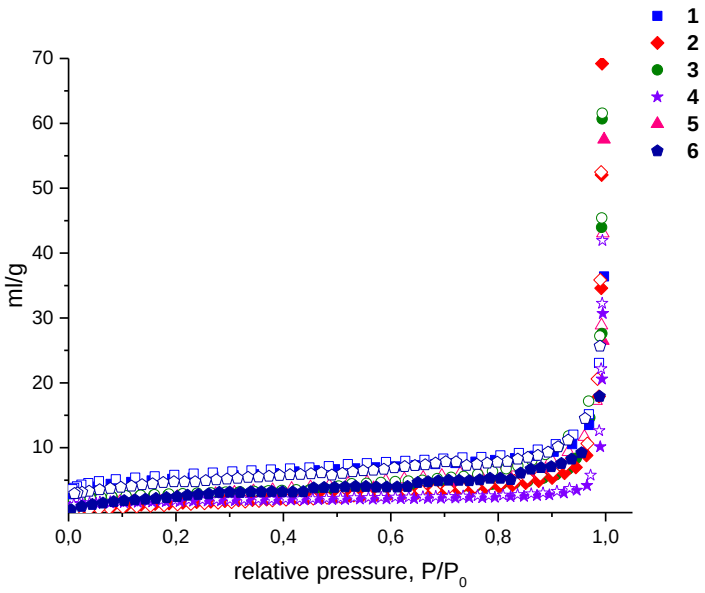

Figure S25. N_2 adsorption isotherms for activated **1**–**6**.

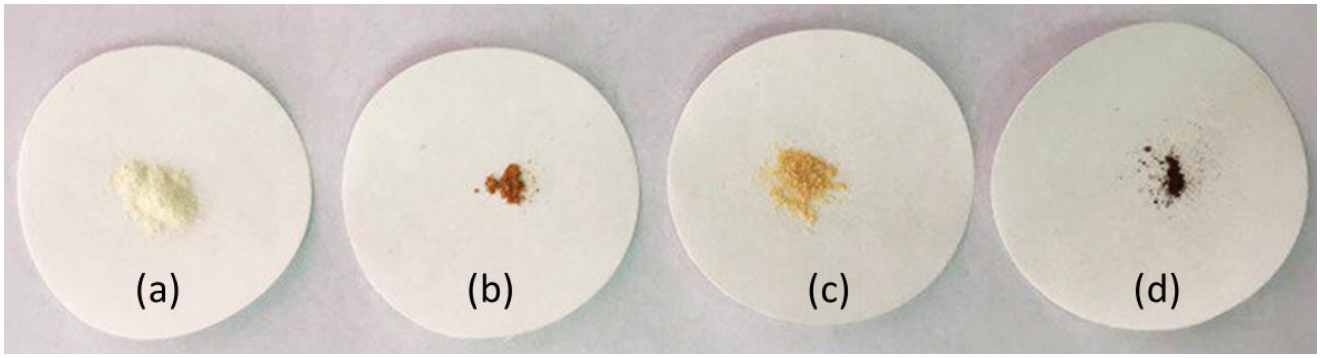

Figure S26. Photos of activated **2** (*a*) and samples soaked in I_2 solution in methanol (*b*), toluene (*c*) and CH_2Cl_2 (*d*) for 1 day.

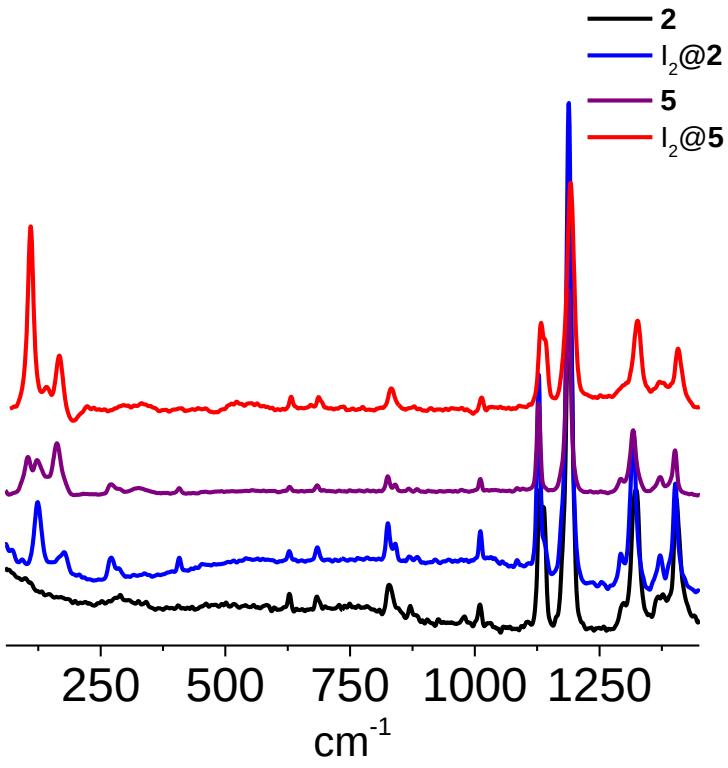

Figure S27. Raman spectra of **2**, **5** and I_2-adsorbted **2** and **5**.

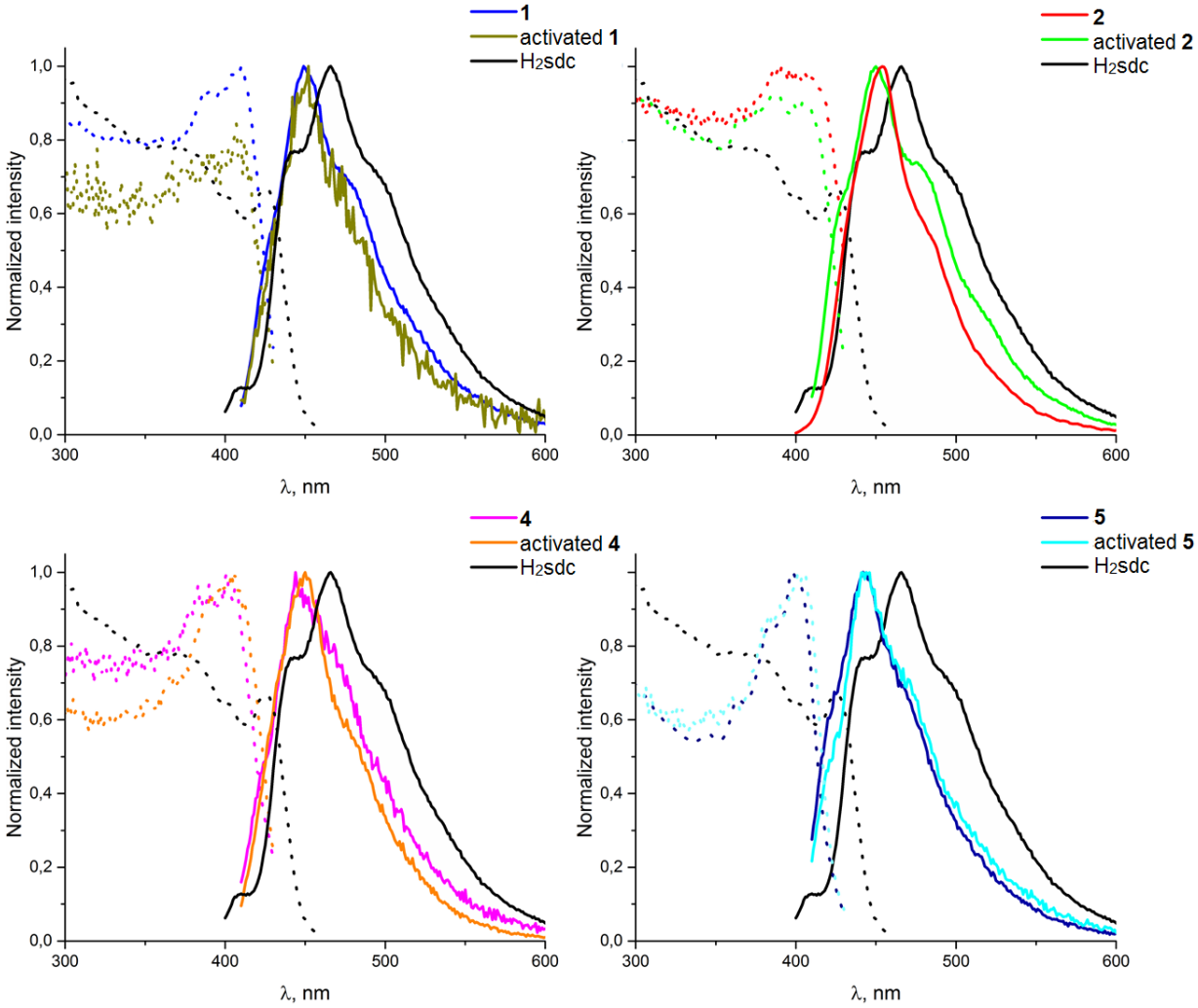

Figure S28. Normalized solid-state luminescence spectra of compounds **1**, **2**, **4**, **5** their activated compounds, and stilbenedicarboxylic acid recorded at λ_{ex} = 390 nm.

Table S1. Chart of MOFs and MOF-based host-guest systems exhibiting high luminescence quantum yields

Compound name/Formula	Quantum yield φ, %	Emission maximum wavelength, nm	Excitation wavelength, nm	Reference
$[NH_2Me_2][(Cd_2Cl)_3(TATPT)_4]$ $[Ir(ppy)_2(bpy)][(Cd_2Cl)_3(TATPT)_4]$	15.1 28.7	425 530	370 370	1
EuN-BDC/m2hmp	31.6	620	370	2
$[Eu(Dpmd)(D_2O)]$	45	5D0	392	3
MOF-253	33	white CCT 5627	395	4
$Zn_2(H_2L)_2(bpy)_2(H_2O)_3 \cdot H_2O$	43	484	376	5
ZrBDC-TCPE0.01%	59	461	363	6

LMOF-231(activated) LMOF-241(activated) LMOF-251	95.1 92.7 90.7		365 340 400	7
Zn-PLA	46%	410	350	8
ZnBDCA	53a	410	360	9
[Zn_2(bpdc)$_2$BTyTPE)]	99	490	365	10
2 **DMF@2**	70.9 82.0			This work

[a] quantum effeciency

Table S2. Crystal data and structure refinement for 1-6.

	1	**2**	**3**	**4**	**5**	**6**
Formula	$C_{29}H_{31}CdN_5O_5$	$C_{29}H_{31}N_5O_5Zn$	$C_{29}H_{31}CoN_5O_5$	$C_{59}H_{63}Cd_2N_9O_9$	$C_{28}H_{28}N_4O_4Zn$	$C_{28}H_{28}CoN_4O_4$
Formula weight	641.99	594.96	588.52	1266.98	549.91	543.47
Crystal system	Monoclinic	Monoclinic	Monoclinic	Orthorhombic	Orthorhombic	Orthorhombic
Space group	*P*2/*c*	*P*2/*c*	*P*2/*c*	$P2_12_12_1$	*Pbcn*	*Pbcn*
a, Å	11.2374(3)	11.5569(8)	11.4594(3)	8.8758(2)	8.6880(4)	8.7112(7)
b, Å	6.78252(13)	6.8510(5)	6.5882(2)	24.0175(7)	14.6001(6)	14.5251(18)
c, Å	18.7482(4)	17.4990(9)	18.3365(5)	28.4657(9)	23.4501(11)	23.5166(18)
β, °	91.4013(19)	92.086(7)	92.145(3)	90.0	90.0	90.0
Z	2	2	2	4	4	4
V, Å^3	1428.52(6)	1384.59(16)	1383.39(7)	6068.2(3)	2974.5(2)	2975.6(5)
θ range, °	3.51 − 26.36	3.46 − 25.35	3.29 − 25.68	3.43 − 25.35	3.47 − 25.35	3.47 − 25.35
Crystal size, mm	0.13×0.09×0.06	0.43×0.13×0.11	0.44×0.14×0.07	0.39×0.16×0.14	0.28×0.20×0.08	0.37×0.20×0.15
D_c, g cm^{-3}	1.493	1.427	1.413	1.387	1.228	1.213
μ, mm^{-1}	0.811	0.935	0.668	0.761	0.862	0.613
Reflections collected/ unique	11382/2920	5825/2536	6164/2601	30671/11071	7843/2724	8674/2731
Reflections with $I > 2\sigma(I)$	2530	1817	2157	9566	2037	2313
R_{int}	0.0225	0.0300	0.0214	0.0350	0.0245	0.0296
GOF on F^2	1.101	1.077	1.084	1.085	1.063	1.200

R_1, wR_2 [$I > 2\sigma(I)$]	0.0260, 0.0609	0.0654, 0.1802	0.0404, 0.1032	0.0768, 0.1875	0.0805, 0.2273	0.1377, 0.3542
R_1, wR_2 (all data)	0.0338, 0.0641	0.0884, 0.1969	0.0526, 0.1094	0.0875, 0.1932	0.1037, 0.2496	0.1512, 0.3638
$\Delta\rho_{max}$/ $\Delta\rho_{min}$,eÅ^{-3}	0.527/−0.353	0.394/−0.613	0.470/−0.283	3.769/−1.021	0.897/−0.510	0.830/−0.499

References

1. Sun, C.-Y.; Wang, X.-L.; Zhang, X.; Qin, C.; Li, P.; Su, Z.-M.; Zhu, D.-X.; Shan, G.-G.; Shao, K.-Z.; Wu, H.; Li, J. Efficient and tunable white-light emission of metal–organic frameworks by iridium-complex encapsulation. *Nat. Commun.* **2013**, *4*, 2717.
2. Kyprianidou, E. J.; Lazarides, T.; Kaziannis, S.; Kosmidis, C.; Itskos, G.; Manos, M. J.; Tasiopoulos, A. J. Single crystal coordinating solvent exchange as a general method for the enhancement of the photoluminescence properties of lanthanide MOFs. *J. Mater. Chem. A* **2014**, *2*, 5258.
3. Vilela, S. M. F.; Ananias, D.; Fernandes, J. A.; Silva, P.; Gomes, A. C.; Silva, N. J. O.; Rodrigues, M. O.; Tomé, J. P. C.; Valente, A. A.; Ribeiro-Claro, P.; Carlos, L. D.; Rocha, J.; Almeida Paz, F. A. Multifunctional micro- and nanosized metal–organic frameworks assembled from bisphosphonates and lanthanides. *J. Mater. Chem. C* **2014**, *2*, 3311.
4. Lu, Y.; Yan, B. Lanthanide organic–inorganic hybrids based on functionalized metal–organic frameworks (MOFs) for a near-UV white LED. *Chem. Commun.* **2014**, *50*, 15443.
5. Deng, Y.; Chen, N.; Li, Q.; Wu, X.; Huang, X.; Lin, Z.; Zhao, Y. Highly fluorescent metal–organic frameworks based on a benzene-cored tetraphenylethene derivative with the ability to detect 2,4,6-Trinitrophenol in water. *Cryst. Growth Des.* **2017**, *17*, 3170.
6. Feng, X.; Zeng, L.; Zou, D.; Zhang, Z.; Zhong, G.; Peng, S.; Liu, L.; Chen, L.; Zhang, J. Trace-doped metal–organic gels with remarkably enhanced luminescence. *RSC Adv.* **2017**, *7*, 37194.
7. Lustig, W. P.; Wang, F.; Teat, S. J.; Hu, Z.; Gong, Q.; Li, J. *Inorg. Chem.* **2016**, *55*, 7250.
8. Chandrasekhar, P.; Mukhopadhyay, A.; Savitha, G.; Moorthy, J. N. Remarkably selective and enantiodifferentiating sensing of histidine by a fluorescent homochiral Zn-MOF based on pyrene-tetralactic acid. *Chem. Sci.* **2016**, *7*, 3085.
9. Cai, H.; Xu, L.-L.; Lai, H.-Y.; Liu, J.-Y.; Ng, S. W.; Li, D. A highly emissive and stable zinc(II) metal–organic framework as a host–guest chemopalette for approaching white-light-emission. *Chem. Commun.* **2017**, *53*, 7917.
10. Tao, C.-L.; Chen, B.; Liu, X.-G.; Zhou, L.-J.; Zhu, X.-L.; Cao, J.; Gu, Z.-G.; Zhao, Z.; Shena, L.; Tang, B. Z. A highly luminescent entangled metal–organic framework based on pyridine-substituted tetraphenylethene for efficient pesticide detection. *Chem. Commun.* **2017**, *53*, 9975.